JOURNAL OF THE MECHANICAL BEHAVIOR OF BIOMEDICAL MATERIALS 61 (2016) 581–589

Available online at www.sciencedirect.com

ScienceDirect

www.elsevier.com/locate/jmbbm

Research Paper

Application of porous titanium in prosthesis production using a moldless process: Evaluation of physical and mechanical properties with various particle sizes, shapes, and mixing ratios

Widyasri Prananingrum[a], *Yoritoki Tomotake*[b,*], *Yoshihito Naito*[b], *Jiyoung Bae*[c], *Kazumitsu Sekine*[c], *Kenichi Hamada*[c], *Tetsuo Ichikawa*[a]

[a]*Department of Oral and Maxillofacial Prosthodontics and Oral Implantology, Institute of Biomedical Sciences, Tokushima University Graduate School, Tokushima, Japan*
[b]*Oral Implant Center, Tokushima University Hospital, Tokushima, Japan*
[c]*Department of Biomaterials and Bioengineering, Institute of Biomedical Sciences, Tokushima University Graduate School, Tokushima, Japan*

ARTICLE INFO

Article history:
Received 29 November 2015
Received in revised form
28 March 2016
Accepted 12 April 2016
Available online 19 April 2016

ABSTRACT

The prosthetic applications of titanium have been challenging because titanium does not possess suitable properties for the conventional casting method using the lost wax technique. We have developed a production method for biomedical application of porous titanium using a moldless process. This study aimed to evaluate the physical and mechanical properties of porous titanium using various particle sizes, shapes, and mixing ratio of titanium powder to wax binder for use in prosthesis production. CP Ti powders with different particle sizes, shapes, and mixing ratios were divided into five groups. A 90:10 wt% mixture of titanium powder and wax binder was prepared manually at 70 °C. After debinding at 380 °C, the specimen was sintered in Ar at 1100 °C without a mold for 1 h. The linear shrinkage ratio of sintered specimens ranged from 2.5% to 14.2%. The linear shrinkage ratio increased with decreasing particle size. While the linear shrinkage ratio of Groups 3, 4, and 5 were approximately 2%, Group 1 showed the highest shrinkage of all. The bending strength ranged from 106 to 428 MPa under the influence of porosity. Groups 1 and 2 presented low porosity followed by higher strength. The shear bond strength ranged from 32 to 100 MPa. The shear bond strength was also particle-size dependent. The decrease in the porosity increased the linear shrinkage ratio and bending strength. Shrinkage and mechanical strength required for prostheses were dependent on the particle size and shape of titanium powders. These findings suggested that this production method can be applied to the prosthetic framework by selecting the material design.

*Corresponding author.
E-mail address: tomotake.dent@tokushima-u.ac.jp (Y. Tomotake).

http://dx.doi.org/10.1016/j.jmbbm.2016.04.021
1751-6161/

1. Introduction

Titanium is widely used in dental implants and artificial joints because of its excellent biocompatibility. However, the elastic modulus of titanium is larger than that of bones (Niinomi, 2002). Titanium with low Young's modulus has been proven effective for inhibiting bone atrophy (Niinomi and Nakai, 2011). For the improvement of elastic modulus of titanium as a bone substitute material, introduction of pores into titanium is effective. We have developed a new production method for application of porous titanium (Naito et al., 2013). This method can provide a favorable elastic modulus by changing the porosity to obtain a similar property to that of the bone.

While titanium can be used for dental implants, its use in prosthesis has been limited because the conventional casting technique for titanium is made challenging by its high melting point and the risk of oxidation (Jorge et al., 2013). Recently, titanium using CAD/CAM systems have been developed as a framework material for implant superstructures. The titanium frame, designed on a PC, is fabricated by shaving out titanium ingots using a milling machine. The CAD/CAM production involves three steps: capturing digital data by scanning a working model or pre-designed frame model, CAD modeling, and CAM production (Drago and Howell, 2012; Abduo and Lyons, 2013). Thus, this process requires equipment, operation technology, and time. Selective laser sintering or selective laser melting offers the advantage of using titanium powder to produce a metal framework, due to its rapid manufacturing rate; a short-term clinical study reported promising outcomes for posterior crowns (Abduo et al., 2014). However, it is difficult to modify the surface of titanium frame after modeling (Abduo et al., 2014), since few correction methods are available for application in clinical settings. Hence, a new manufacturing process is required for application of titanium in prosthesis production.

This study focuses on the production method of porous titanium that we have developed, and on its validity for prosthesis application. Fig. 1 shows the framework of the implant prosthesis manufactured using this method with the copings of the titanium product as a preliminary fabrication. It should be noted that this method can bond the titanium powders to the copings of the titanium product. The basic requirements for a prosthesis to achieve acceptable longevity are a precision fit to the abutment, mechanical strength against the occlusal force, and technical operability. The accurate fit of the prosthesis to the abutments is affected by the shrinkage of prosthetic materials. In the casting process of the conventional lost wax technique, metal prostheses are controlled to compensate for dimensional accuracy by adjusting the expansion and contraction of multiple materials. The mechanical strength of the prosthesis is important to withstand the occlusal force of mastication or parafunction to prevent failure (Agustin-Panadero et al., 2014). The production method using a moldless process enables a simple manufacturing process that produces a mixture of high formability without using a mold and a conventional casting operation. This method can adjust the porosity, shrinkage and mechanical properties of the porous titanium by changing the sintering condition (Naito et al., 2013). Furthermore, the mechanical properties of sintered body do not depend only on the sintering condition, but also the microstructure of the initial powder (Wang et al., 2010; Chaiyabutr et al., 2009; Chen et al., 2008). Thus, it is also necessary to clarify the specific properties of porous titanium with different types of powder in this production method.

Therefore, this study aimed to evaluate the physical and mechanical properties of porous titanium using a moldless process with various particle sizes, shapes, and mixing ratio of titanium powder, for application in prosthesis production.

2. Materials and methods

2.1. *Preparation of materials*

Three different kinds of commercially pure titanium powder were used in this study: Ti powder diameter $<45\,\mu m$ in irregular shape (Nilaco Co., Tokyo, Japan), $<45\,\mu m$ in spherical shape (Osaka Titanium Technologies Co, Hyogo, Japan), and $<150\,\mu m$ in spherical shape (Osaka Titanium Technologies). As shown in Table 1, five types of Ti/wax mixtures were prepared as follows: Ti $<45\,\mu m$ in irregular shape 90 wt% (Group 1), Ti $<45\,\mu m$ in spherical shape 90 wt% (Group 2), Ti $<150\,\mu m$ in spherical shape 90 wt% (Group 3), mixed powder consisting of 75 wt% Ti $<150\,\mu m$ in spherical shape and 15 wt% Ti $<45\,\mu m$ in irregular shape (Group 4), and mixed powder consisting of 80 wt% Ti $<150\,\mu m$ in spherical shape and 10 wt% Ti $<45\,\mu m$ in irregular shape (Group 5). The particle size distribution was determined with a particle size analyzer (Horiba CAPA-300, Kyoto, Japan). Group 1 and Group 2 were measured by diluting 0.05 g of powder in 50% glycerol solution. Groups 3, 4 and 5 were measured by diluting 0.1 g of powder in 50% glycerol solution (Segur and Oberstar, 1951). The sintering result of each specimen was observed using a scanning electron microscope (JSM-5300, JEOL, Tokyo, Japan).

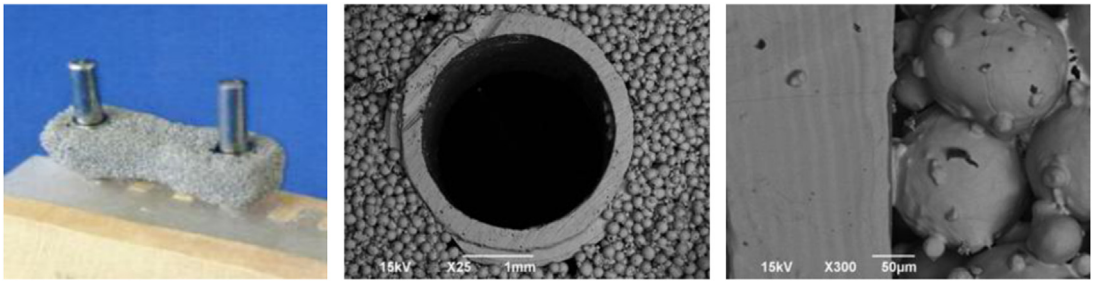

Fig. 1 – The bonding of titanium powder to the coping of titanium product.

2.2. The production method of porous titanium

Porous titanium was produced according to the method presented by Naito et al. (2013). Fig. 2 shows the procedure of this production method.

Titanium powder and inlay casting wax binder (custom ordered colorless type I; GC Corporation, Tokyo, Japan) were mixed in a ratio of 90:10 wt% at 70 °C on a hot plate. Then, the powder and wax mixture was poured into a silicone mold at room temperature. The top surface was flattened with spatula. After slow cooling, the green bodies were heated in air at a rate of 20 °C/min up to 380 °C in a furnace (GC Autofurnace FM-X, GC Dental Industrial Corp., Tokyo, Japan) for 2 h without a mold, to remove the binder. The sintering process was conducted in an argon atmosphere at a heating rate of 10 °C/min to 1100 °C for 1 h (Furnace BDK-1S-0, Miwa MFG Co. LTD, Osaka, Japan). After slow cooling, the specimens were ultrasonically cleaned with acetone, ethanol, and distilled water for 10 min, sequentially. Then, the rinsed specimens were dried in a desiccator overnight. Six specimens were prepared in each test.

2.3. Density of the green body

The specimens with a diameter of 3 mm and height of 4 mm were prepared. The green body was weighed using an analytical balance (AUW220D, Shimadzu, Kyoto, Japan). The density was calculated using the following equation:

$$d = mass/volume$$

where d is the density (kg/m^3), *mass* is the green body weight (kg), and *volume* is the volume of the specimen (m^3).

Table 1 – Mixing ratio of titanium powder and wax binder.

	Titanium powder (mass%)			Wax (mass%)
	<45 μm (irregular shape)	<45 μm (spherical shape)	<150 μm (spherical shape)	
Group 1	90	–	–	10
Group 2	–	90	–	10
Group 3	–	–	90	10
Group 4	75	–	15	10
Group 5	80	–	10	10

2.4. Linear shrinkage ratio

The linear shrinkage ratio was evaluated using a laser displacement sensor (LK-G155, Keyence, Osaka, Japan) at room temperature. The specimens with a diameter of 3 mm and height of 4 mm were used for the evaluation. The height of each specimen was measured five times each before and after the sintering process, and the average value was obtained. The linear shrinkage ratio was calculated using the following equation:

$$S = (H_0 - H_1)/H_0 \times 100$$

where S is the linear shrinkage ratio (%), H_0 is the specimen height before sintering (mm), and H_1 is the specimen height after sintering (mm).

2.5. Porosity

The porosity of the specimens after sintering was measured according to the method presented by Semel and Lados (2006). The total porosity was evaluated on the basis of the apparent volume calculated from the specimen dimensions, while the actual volume evaluated using helium pycnometry (Accupyc II 1340, Micromeritics Instrument Corp., Norcross, GA) at room temperature. The open and closed porosities were calculated from 3D reconstruction using the micro-computed tomography (SkyScan 1176, Bruker Micro-CT, Kontich, Belgium). Open porosity is defined as a percent of the total VIO volume. Closed porosity represents the volume of the closed pores as a percent of total solid plus closed pore volume within the VOI. The specimens with a diameter of 3 mm and height of 4 mm were used for the evaluation.

2.6. Bending strength

The rectangular specimens (14 × 4 × 2 mm) were prepared following the production method for porous titanium as it mention above. The mechanical properties of fabricated specimens after sintering were evaluated with a three-point bending test using a universal testing machine (AG-X, Shimadzu Corp., Tokyo, Japan) with a crosshead speed of 0.5 mm/min, at room temperature. The conditions of the test were that the bending span was 10 mm, and an indenter with a 3-mm tip diameter was used. The bending strength was determined using the following equation:

$$\sigma = 3PL/2bh^2$$

where σ is the bending strength (Pa), P is the load at fracture (N), L is the span length (m), b is the specimen width (m), and

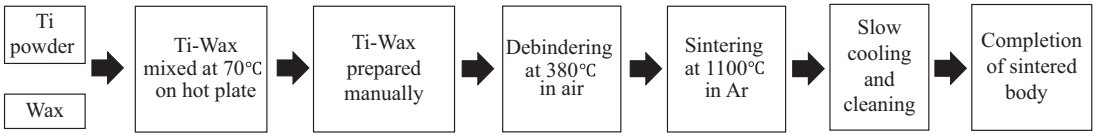

Fig. 2 – The procedure of moldless process.

h is the specimen thickness (m). The fractured surface of the specimens was observed using SEM.

2.7. Shear bond strength

The interfacial adhesion between porous titanium (d 3 mm, h 4 mm) and bulk titanium plate ($10 \times 10 \times 1$ mm) (99.5% in purity) was evaluated through shear bonding strength test, due to the application of the porous titanium with prefabricated cylinder of the framework component. The mixture of titanium powder and wax was injected on the bulk titanium plate manually at 70 °C on the hot plate. Fig. 3 shows a schematic diagram of the test procedure. The shear bond strength was evaluated under compressive loading at a crosshead speed of 0.5 mm/min using a universal testing machine at room temperature. The shear bond strength was calculated by dividing the peak load values by the sintered specimen base area. The fractured surfaces and the mode of fracture were observed using SEM.

2.8. Statistical analysis

Statistical analysis was performed by One-Way ANOVA followed by a Tukey post hoc test for multiple comparisons using SPSS (SPSS Inc., Chicago, IL, USA). Statistical significance was set at the 95% level.

3. Results

3.1. Particle size distribution

The particle size distribution was shown in Fig. 4. Groups 1 and 2 were distributed in the range 0–25 μm and 0–45 μm, respectively. Meanwhile, the particle size of Groups 3, 4 and 5 showed the distribution in the 0–110 μm range. It could not detailed in specific of particle size over 110 μm for the performance of the device, but the proportion of them is small.

3.2. SEM images

Fig. 5 shows the sintering result of each specimen group. The necking among titanium powders was observed on the upper surface of the specimen. In Group 1, it can be seen that the necking growth resulted in near full dense surface while there was a slightly gaps. In Group 2, some gaps were shown in comparing with Group 1. For Group 3 composed of the large particles without the small particles, Groups 4 and 5 showed that the small particles filled the gaps between the large particles and reduce interparticle gaps.

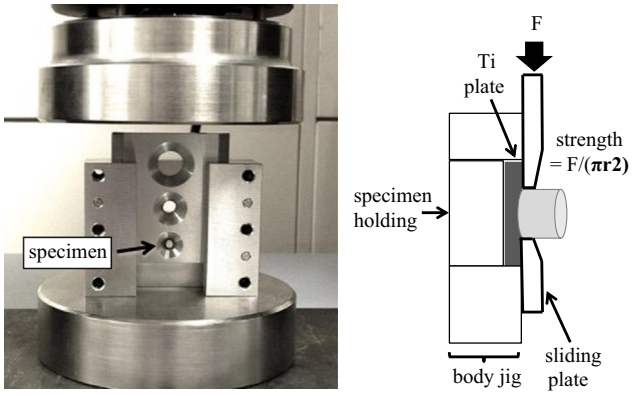

Fig. 3 – Shear bond strength measurement.

3.3. Linear shrinkage ratio

Fig. 6 shows the linear shrinkage ratio of the sintered specimens in the 2.5–14.2% range. The linear shrinkage ratio in Group 1 was significantly higher than that in other groups. Groups 3, 4, and 5 showed significantly lower values compared to Groups 1 and 2. There was no significant difference in the linear shrinkage ratios among Groups 3, 4, and 5.

3.4. Density and porosity

The density of the green body is shown in Fig. 7. The density in Group 1 was significantly lower than that in the other groups. While there was no significant difference between values for Groups 2 and 3, the density of the green body in Group 3 was significantly lower than that in Groups 4 and 5. There was no significant difference between densities in Groups 4 and 5. The porosity of the sintered specimen is shown in Fig. 8. The samples demonstrated varying porosity ranging from 17.7% to 38.5%. The open and closed porosities were in the 17–38% and 0–0.8% ranges, respectively (Table 2). Group 1 showed significantly lower porosity compared with that in the other groups. While there was no significant difference between porosities in Groups 2 and 4, there was a significant difference between Groups 2 and 5. The porosity in Group 3 was significantly higher than that in the other groups.

3.5. Bending strength

Fig. 9 shows the bending strength of each group. The bending strength in Group 1 was significantly higher than that in Groups 3, 4 and 5. There was no significant difference in bending strength between Groups 1 and 2.

3.6. Shear bond strength

The shear bond strength is shown in Fig. 10. The shear bond strength of Group 1 was significantly higher compared to that of Groups 3 and 4. On the other hand, there was no significant difference among Groups 1, 2, and 5. Figs. 11 and 12 show the fractured surface of the specimens after the shear bond strength test. The fracture mode was cohesive for all the groups. The fracture occurred within the sintered body close to the interface between bulk titanium plate and porous titanium.

4. Discussion

The results of the present study clarified the physical and mechanical properties of porous titanium using a moldless

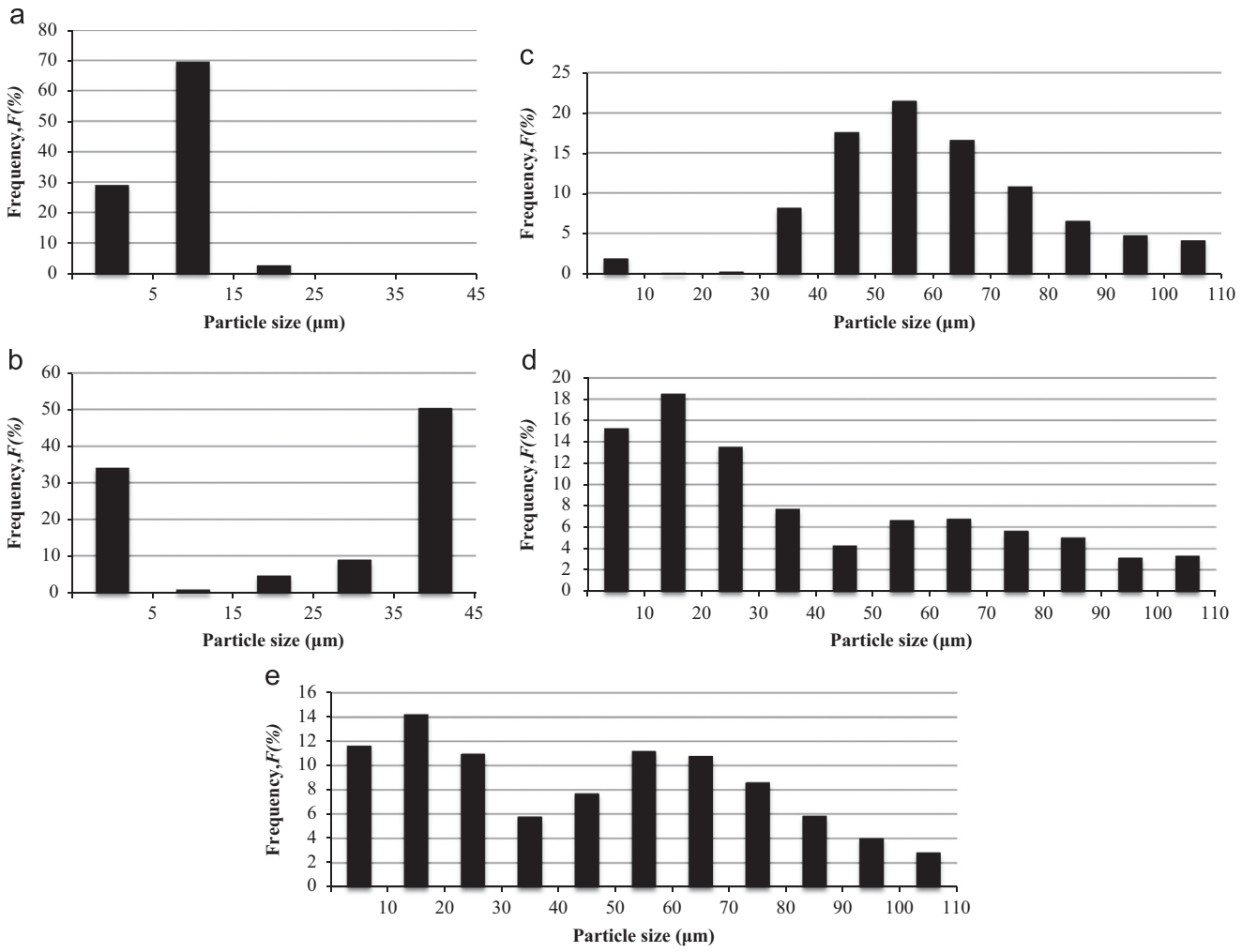

Fig. 4 – Particle size distribution of titanium powder (a) Group 1, (b) Group 2, (c) Group 3, (d) Group 4 and (e) Group 5.

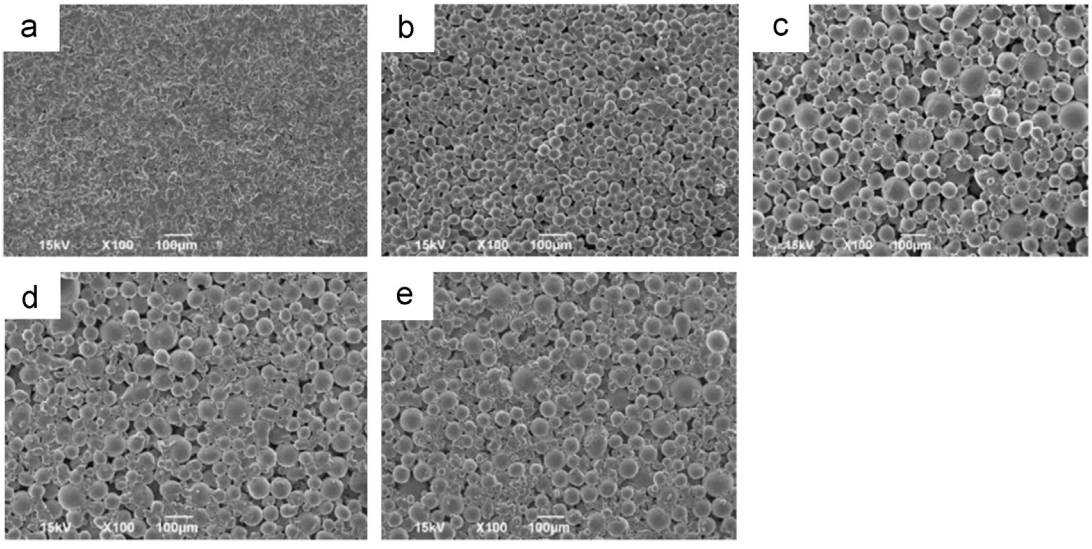

Fig. 5 – Scanning electron microscope (SEM) images show the necking of titanium powder in the upper surface after sintering process (a) Group 1, (b) Group 2, (c) Group 3, (d) Group 4 and (e) Group 5.

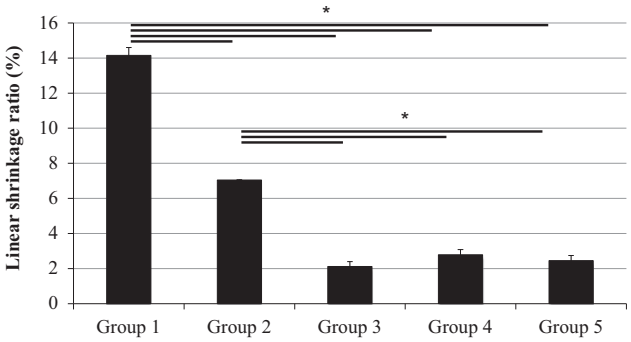

Fig. 6 – Linear shrinkage ratio of the sintered specimens (*$p<0.05$).

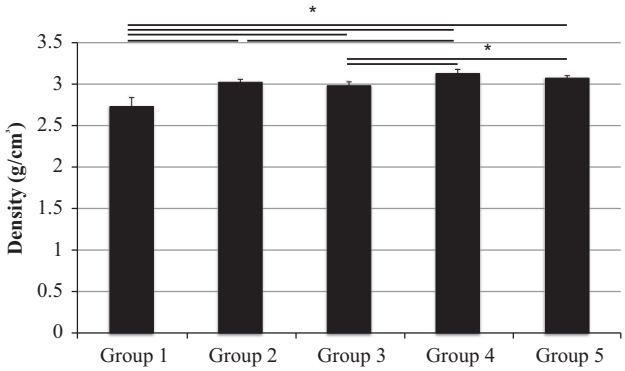

Fig. 7 – Density of the green bodies (*$p<0.05$).

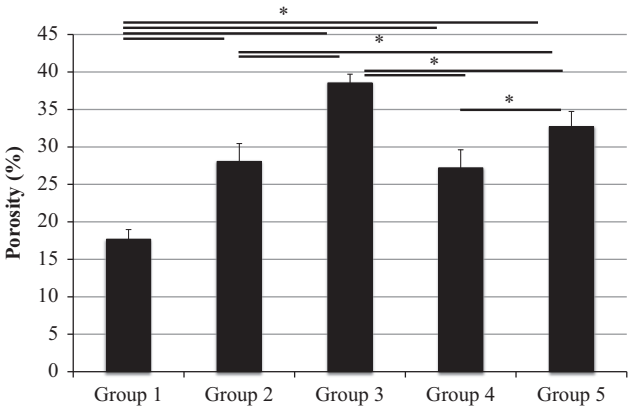

Fig. 8 – Porosity of the sintered specimens (*$p<0.05$).

process with various particle sizes, shapes, and mixing ratios of titanium powder, for application in prosthesis production.

As seen in the SEM image (Fig. 5), titanium powders were bound together after the sintering process. The physical and mechanical properties are hypothesized to be dependent on the microstructure, which is determined by the differences in the powders. The initial type of CP Ti powder contributes to the diversity of the microstructure. Groups 1 and 2 presented a narrow particle size distribution. On the other hand, a broad size distribution was presented in Groups 3, 4 and 5 (Fig. 4). The linear shrinkage ratio of sintered specimens was in the

Table 2 – The open and closed porosities of sintered specimen.

Open porosity (%)	Closed porosity (%)
17	0
26	0.1
38	0.8
27	0.4
31	0.3

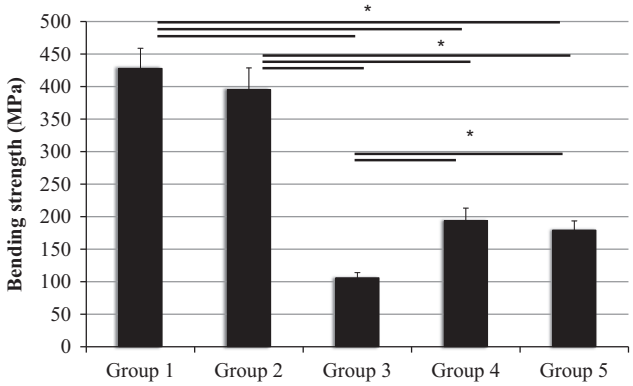

Fig. 9 – Bending strength of the sintered specimens (*$p<0.05$).

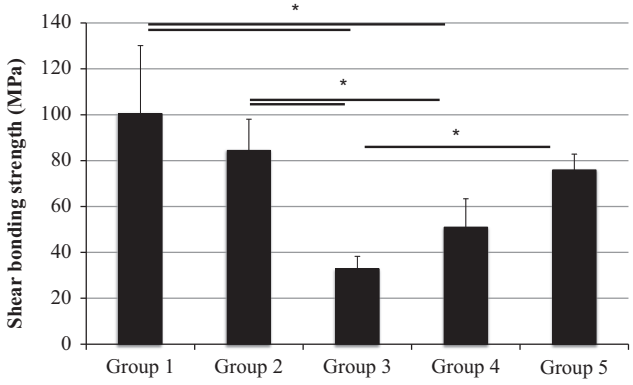

Fig. 10 – Shear bond strength of the sintered specimens (*$p<0.05$).

range of 2.5–14.2%. The linear shrinkage ratio increased with the decreasing particle size. All base metal alloys used for dental application shrink by 2.0–2.3% upon solidification; for example, Co–Cr alloys exhibit a 2.3% shrinkage rate and Ni–Cr alloys exhibit a 2.0% shrinkage rate (Anusavice et al., 2012). The linear shrinkage ratio of Groups 3, 4, and 5 were approximately 2%, which was similar to that for the above cast metals. Group 1 showed the highest shrinkage. This can be explained by the fact that small particles have a much higher surface energy, and are therefore, easy to sinter (Oh et al., 2003). The particle size of Group 2 was similar to that in Group 1, but the linear shrinkage ratio was significantly lower compared to that in Group 1. It suggested that shrinkage behavior strongly depends on the particle shape. The irregular-shaped particles showed high shrinkage ratios

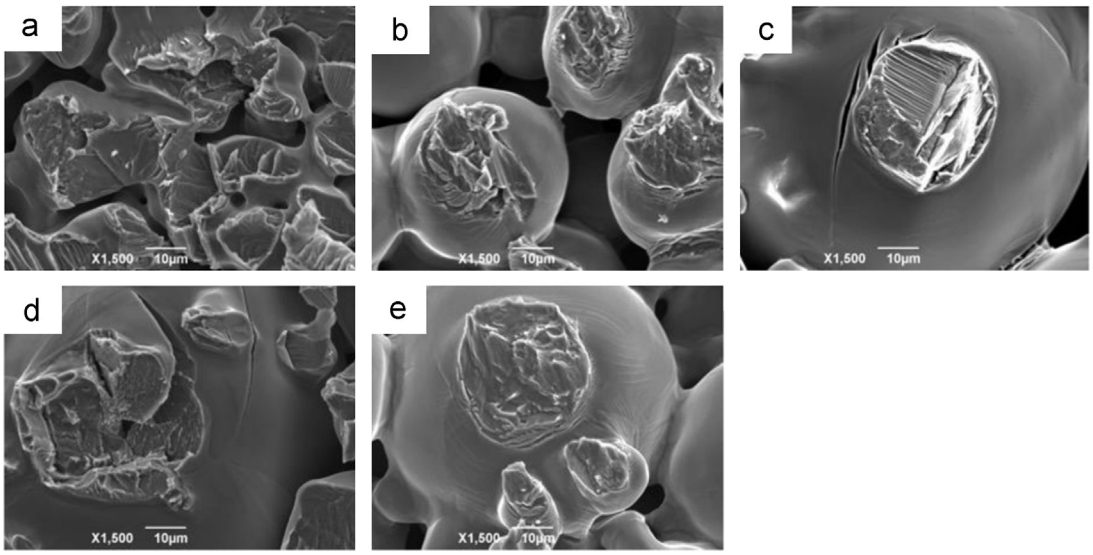

Fig. 11 – SEM images of the fracture surface of sintered specimens after shear bond strength test (a) Group 1, (b) Group 2, (c) Group 3, (d) Group 4 and (e) Group 5.

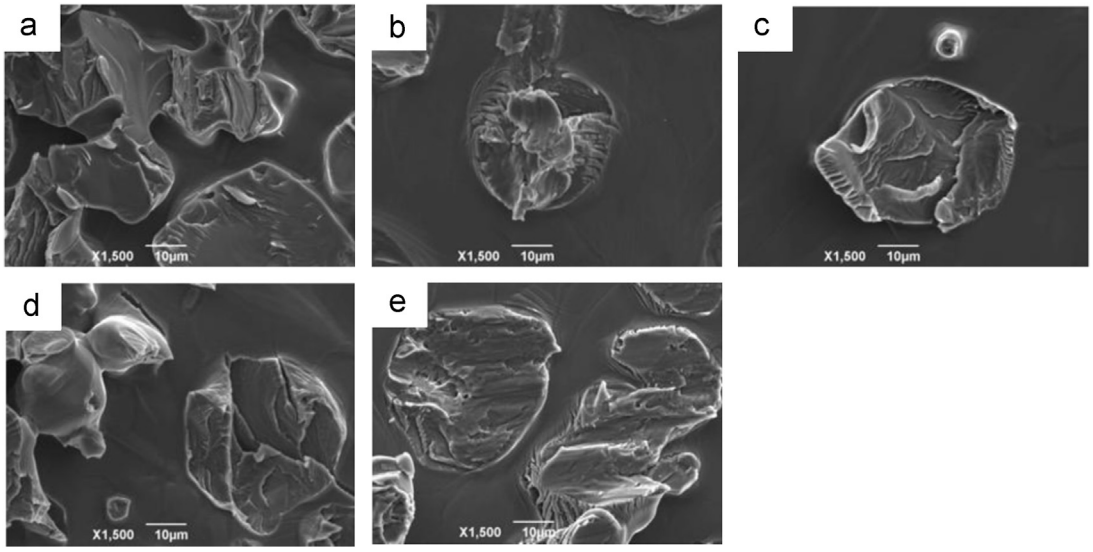

Fig. 12 – SEM images of the fracture surface of titanium plate after shear bond strength test (a) Group 1, (b) Group 2, (c) Group 3, (d) Group 4 and (e) Group 5.

compared to the spherical-shaped ones because of low green body density related to poor packing property of the powder (Figs. 6 and 7). This result suggested that the irregular morphology of powder increased shrinkage ratio. This finding is in agreement with that of Koseski et al. (2005), where lower green density of irregular stainless steel powder resulted in an increased sintering shrinkage rate. As shown in Fig. 7, substitution of irregular small particles for spherical large particles resulted in an increase in the green body density. On the other hand, the linear shrinkage ratios of Groups 3, 4, and 5 were nearly equal.

In this study, the porosity ranged from 17.7% to 38.5%. The smallest particle size specimens showed the lowest porosity. In contrast, the largest particle size specimens showed the highest porosity. The irregular small particle size results in lower green density and higher surface area, therefore the porosity decreased quickly at the same sintering condition. Meanwhile, the specimen with substitution of the small size particles for large size particles with 15 mass% (Group 4) showed significantly lower porosity than that of 10 mass% substitution specimens (Group 5) and no substitution specimens (Group 3). As seen in Fig. 5, the small particles fill the spaces between the large particles and reduce interparticle spacing. These results suggested that particle size and mixing ratio play an important role in the porosity and the pore morphology. The results of micro-computed tomography analysis showed that the porosities of all the groups were almost open porosity (Table 2). It suggested that more pores are interconnected. Within limitation of this study, it is difficult to control the pore shape. Although some spherical pores were observed in Group 1, but some irregular shape

were also found and the pores were not uniformly distributed (Fig. 5).

With respect to the mechanical properties of the prosthetic materials, three-point bending strength of porous titanium using moldless process was evaluated. In this study, the bending strength was in the range 106–428 MPa, which was less than the value for cast titanium. Cast titanium presented a bending strength ranged from 590 to 925 MPa, depending on the investment material and mold temperature (Rodrigues et al., 2012; Lin et al., 2004). Meanwhile, the bending strength of zirconia ranged from 586 to 1281 MPa, depending on the sintering temperature (Stawarcyk et al., 2013). Group 1 presented the lowest porosity and highest bending strength. In contrast Group 3 presented the highest porosity and lowest bending strength (Figs. 8 and 9). These results indicate that the porosity of porous titanium was associated with the bending strength.

Several studies have described the possibility of bonding the framework to prefabricated framework implant cylinder (Jackson, 2005; Yoshinari et al., in press). The noteworthy advantage of this production method of porous titanium using a moldless process might be the bonding of porous titanium to the ready-made titanium framework components. The shear bond strength ranged from 32 to 100 MPa, and depended on particle size. This finding was less than the joining titanium using laser welding technique that presented 595 MPa for tensile strength (Iwasaki et al., 2004). Ti $<$ 45 μm showed significantly higher shear bond strength compared to Ti $<$ 150 μm. Regarding the shape of the initial particle, the shear bond strength of specimens using irregular particles was nearly equal to that of the specimens using spherical particles. As shown in Fig. 10, the substitution of small size particles for large size particles improved the shear bond strength. The substitution of small titanium particles for large titanium particles with 10 mass% (Group 5) resulted in significantly lower strength than that in the no substitution group, and slightly higher strength than that in the 15 mass% of substitution specimens (Group 4). The cohesive failure of the porous titanium close to the interface between bulk titanium and porous titanium was observed in all groups in which the failure occurred within the porous titanium without bulk titanium exposure. The SEM images showed the fracture surface of the specimens (Figs. 11 and 12). The images indicated that the plastic deformation could not observe. This finding suggested that the bonding strength between the porous titanium and bulk titanium is high enough to allow application of the porous titanium with a ready-made titanium component. Since the bonding strength is affected by the strength of the fabricated porous titanium itself, this technique can be applied as an improved method to modify the frame surface for veneer retention. Moreover, it provides a correction method to revise the framework shape of prostheses in order to reinforce the occlusal support.

The results of current study suggest that the physical and mechanical properties of porous titanium need to be improved for application in a prosthetic framework. Since Groups 1 and 2 showed the highest mechanical strength and a high linear shrinkage ratio, this method can be applicable for CAD/CAM system usage by controlling the linear shrinkage ratio, as in a zirconia framework. Although it was possible to reduce the linear shrinkage ratio in Groups 3, 4, and 5, similar to that observed with the use of all base metal alloys, the mechanical strengths were insufficient. It is therefore necessary to improve the strengths without the increase of shrinkage rate in order to apply it for prosthesis production.

5. Conclusion

The results of this study clarified the mechanical properties of porous titanium with various particle sizes, shapes, and mixing ratios of titanium powder for the production method of porous titanium using a moldless process for prosthesis production. The decrease in the porosity increased the linear shrinkage ratio and bending strength. Physical and mechanical properties required for prosthesis were dependent on the particle sizes, shapes and mixing ratios of titanium powders. Thus, this production method can be applied to the prosthetic framework by selecting the appropriate material design.

Acknowledgments

This work was partially supported by the Japan Society for the Promotion of Science (JSPS, KAKENHI Grant number 1511196).

REFERENCES

Abduo, J., Lyons, K., 2013. Rationale for the use CAD/CAM technology in implant prosthodontics. Int. J. Dent. 2013, 8.

Abduo, J., Lyons, K., Bennamoun, M., 2014. Trends in computer-aided manufacturing in prosthodontics: a review of available streams. Int. J. Dent. 2014, 5.

Agustin-Panadero, R., Rodriguez, J.L.R., Ferreiroa, A., Ruiz, M.F.S., Font, A.F., 2014. Zirconia in fixed prosthesis. A literature review. J. Clin. Exp. Dent. 6 (1), e66–e73.

Anusavice, K.J., Shen, C., Rawls, H.R., 2012. Phillip's Science of Dental Materials, 12th ed. W.B. Saunders Company, St. Louis199–386.

Chaiyabutr, Y., Giordanio, R., Pober, R., 2009. The effect of different powder particle size on mechanical properties of sintered alumina, resin- and glass-infused alumina. J. Biomed. Mater. Res. Part B: Appl. Biomater. 88B (2), 502–508.

Chen, J.K., Tang, T.P., Chan, S.F., Chang, S.H., 2008. Effects of particle size on mechanical properties of a TiC containing tool steel by hot isostatic press. Mater. Trans. 49 (3), 624–628.

Drago, C., Howell, K., 2012. Concepts for designing and fabricating metal implant frameworks for hybrid implant prostheses. J. Prosthodont. 21 (5), 413–424.

Iwasaki, K., Ohkawa, S., Motohiro, U., Tsukasa, A., Watari, F., 2004. Laser welding of titanium and dental preciouss alloys. Mater. Trans. 45 (4), 1140–1146.

Jackson, B.J., 2005. The use of laser-welded titanium framework technology: a case report for totally edentulous patient. J. Oral Implantol. 31 (6), 294–300.

Jorge, J.R.P., Barão, V.A., Delben, J.A., Faverani, L.P., Queiroz, T.P., Assunção, W.G., 2013. Titanium in dentistry: historical development, state of the art and future perspectives. J. Indian Prosthodont. Soc. 13 (2), 71–77.

Koseski, R.P., Suri, P., German, R.M., Kwon, Y.-S., 2005. Microstructural evolution of injection molded gas- and water-atomized 316L stainless steel powder during sintering. Mater. Sci. Eng. A 390 (1–2), 171–177.

Lin, C.W., Ju, C.P., Lin, J.H.C., 2004. Comparison among mechanical properties of investment-cast c.p. Ti, Ti–6Al–7Nb and Ti–15Mo–1Bi alloys. Mater. Trans. 45 (10), 3028–3032.
Naito, Y., Bae, J., Tomotake, Y., Hamada, K., Asaoka, K., Ichikawa, T., 2013. Formability and mechanical properties of porous titanium produced by a moldless process. J. Biomed. Mater. Res. B Appl. Biomater. 101B (6), 1090–1094.
Niinomi, M., 2002. Recent metallic materials for biomedical applications. Metall. Mater. Trans. A 33 (3), 477–486.
Niinomi, M., Nakai, M., 2011. Titanium-based biomaterials for preventing stress shielding between implant devices and bone. Int. J. Biomater. 2011, 1–10.
Oh, I.K., Segawa, H., Nomura, N., Hanada, S., 2003. Microstructures and mechanical properties of porosity-graded pure titanium compacts. Mater. Trans. 44 (4), 657–660.
Rodrigues, R.C., Almeida, E.P., Faria, A.C.L., Macedo, A.P., Mattos, M.G.C., Ribeiro, R.F., 2012. Effect of different investments and mold temperatures on titanium mechanical properties. J. Prosthodont. Res. 56 (1), 58–64.
Segur, J.B., Oberstar, H.E., 1951. Viscosity of glycerol and its aqueous solutions. Ind. Eng. Chem. 43 (9), 2117–2120.
Semel, F.J., Lados, D.A., 2006. Porosity analysis of PM materials by helium pycnometry. Powder Metall. 49 (2), 173–182.
Stawarcyk, B., Özcan, M., Hallmann, L., Ender, A., Mehl, A., Hämmerlet, C.H.F., 2013. The effect of zirconia sintering temperature on flexural strength, grain size and contrast ratio. J. Clin. Oral. Invest. 17 (1), 269–274.
Wang, H., Fang, Z.Z., Sun, P., 2010. A critical review of mechanical properties of powder metallurgy titanium. Int. J. Powder Metall. 46 (5), 45–57.
Yoshinari, M., Uzawa, S., Komiyama, Y., 2016. Hybrid framework with cobalt–chromium alloy and gold cylinder for implant superstructure: bond strength and corrosion resistance. J. Prosthodont. Res. (in press).